Spectral Diffusion Map Approach for Structural Health Monitoring of Wind Turbine Blades

V. Chinde, L. Cao , U. Vaidya, and S. Laflamme

Abstract— **In this paper, we develop data-driven method for the diagnosis of damage in mechanical structures using an array of distributed sensors. The proposed approach relies on comparing intrinsic geometry of data sets corresponding to the undamage and damage state of the system. We use spectral diffusion map approach for identifying the intrinsic geometry of the data set. In particular, time series data from distributed sensors is used for the construction of diffusion map. The low dimensional embedding of the data set corresponding to different damage level is done using singular value decomposition of the diffusion map to identify the intrinsic geometry. We construct appropriate metric in diffusion space to compare the different data set corresponding to different damage cases. The application of this approach is demonstrated for damage diagnosis of wind turbine blades. Our simulation results show that the proposed diffusion map-based metric is not only able to distinguish the damage from undamage system state, but can also determine the extent and the location of the damage.**

I. Introduction

Structural health monitoring (SHM) of wind turbine blades is a problem that has received increased attention because of the prominent role wind turbine technology plays in the renewable energy future. The size of wind turbines blades has increased over years to harvest large amount of energy economically and efficiently. The inherent large geometrical size of the monitored system impedes the applicability of existing sensing solutions [1], [2]. Because it is well understood that condition assessment of blades may have strong economic benefits [3]–[5], various research efforts have been oriented towards developing sensing systems tailored to this SHM challenge. In particular, dense arrays of sensors have been proposed [2], [6]–[8] to mimic biological skins, where changes in a local state can be monitored over a global area.

In this paper, we develop spectral diffusion map based approach for structural health monitoring of wind turbine blades. The basic idea behind the proposed approach is to compared the intrinsic geometry of the data sets obtained from the undamaged and damaged system state. The intrinsic geometry of the data set is obtained using multiscale diffusion map approach developed in [9]. The diffusion-map method provides an embedding of the time-series data set in the diffusion space to identify important lower dimensional dynamical features of the data. We construct appropriate metric in the diffusion space to compare the embedded data under normal and abnormal operating conditions. The diffusion map-based approach combines ideas from variety of methods currently adopted for data-driven schemes for health monitoring such as spectral graph theory, Kernel methods, and machine learning. One of the important advantages of the proposed diffusion map-based approach is that it can be used for sensor data fusion. We exploit this capability for the development of sensor fusion-based SHM scheme.

The application of data-driven and data-dimensionality based methods for SHM of civil structures is not new [10]–[14]. These applications consist of constructing an attractor of proper dimension and time delay from one or many observations, and studying changes in the phase-space to detect damages. Similarly, diffusion map-based approach has also been to used for detection of anomaly in dynamical systems [15]. A variation of diffusion maps called Discriminant Diffusion Maps Analysis (DDMA) has been used for machine condition monitoring and fault diagnosis [16]. In [17], theoretical basis for construction of diffusion map for changing data set is proposed. The main contribution of this paper is in the application of diffusion map approach for SHM of wind turbine blades. We show that our proposed approach can not only be used for the detection of damage but also for damage localization.

The organization of the paper is as follows. In Section II, we discuss the theory behind the diffusion maps. The application of diffusion maps for the comparison of different data sets and for sensor fusion is discussed in Section III. The wind turbine and wind load modeling is presented in Section IV followed by simulation results in Section V. Conclusions are presented in Section VI.

II. Diffusion maps

In this section, we provide brief overview of diffusion maps. The material for this section is taken from [9], [18]. The construction of diffusion map starts with the construction of kernel function, $k(x, y)$, on set of data points Γ where x and y are data points and belongs to space X. The kernel function $k(x, y)$ is constructed to satisfy following properties.

- k is symmetric, i.e., $k(x, y) = k(y, x)$
- k is positivity preserving i.e., $k(x, y) \geq 0$ for all x, y.
- k is positive semidefinite for all real valued bounded function f defined on data set Γ

$$\int_X \int_X k(x, y) f(x) f(y) d\mu(x) d\mu(y) \geq 0$$

where μ is a probability measure on X

This research work is supported by grant from Iowa Energy Center (IEC). V. Chinde and U. Vaidya are with the Department of Electrical and Computer Engineering. L. Cao and S. laflamme are with the Department of Civil Engineering. Emails: vchinde, ugvaidya, liangcao, laflamme (@iastate. edu)

The kernel function $k(x,y)$ is constructed based on local connectivity of data points and hence capture the local geometry of data set. Several choices for the kernel k are possible all leading to different analyses of data. The idea behind the diffusion map is to construct the global geometry of the data set from the local information contained in the kernel $k(x,y)$. The construction of the diffusion map involves the following steps. First, we normalize the kernel $k(x,y)$ in the graph Laplacian fashion [19] . For all $x \in \Gamma$

$$\text{let} \quad v^2(x) = \int_\Gamma k(x,y)d\mu(y)$$

$$\text{set} \quad \tilde{a}(x,y) = \frac{k(x,y)}{v^2(x)}$$

and $\tilde{a}$ satisfies $\int \tilde{a}(x,y)d\mu(y) = 1$. To $\tilde{a}$ we can associate a random walk operator on the data set Γ as

$$\tilde{A}f(x) = \int \tilde{a}(x,y)f(y)d\mu(y).$$

Since we are interested in the spectral properties of the operator it is preferable to work with a symmetric conjugate of $\tilde{A}$. We conjugate $\tilde{a}$ by v in order to obtain a symmetric form and we consider

$$a(x,y) = \frac{k(x,y)}{v(x)v(y)}$$

and operator

$$Af(x) = \int a(x,y)f(y)d\mu(y).$$

The operator A is referred to as diffusion operator. Under very general hypotheses the operator A is compact and self-adjoint so by spectral theory we have

$$a(x,y) = \sum_{j\geq 0} \lambda_j \varphi_j(x)\varphi_j(y), \quad A\varphi_j(x) = \lambda_j \varphi_j(x).$$

Let $a^m(x,y)$ be the kernel of A^m, then at the level of data points the kernel $a^m(x,y)$ has a probabilistic interpretation as a Markov chain with transition matrix a to reach y from x in m steps. The mapping

$$\Phi(x) = (\varphi_0(x), \varphi_1(x), ..., \varphi_p(x), ...)$$

(where φ_i are the eigenfunctions of diffusion operator A) maps the data set $x \in \Gamma$ into the Euclidean space ($\ell^2(N)$), which we will call the diffusion space. Each eigenfunction can be interpreted as a coordinate on the set. This mapping can be used as a diffusion metric to measure the diffusion distance between the data point $x, y \in \Gamma$. More precisely the diffusion metric can be written as

$$D_m^2(x,y) = \sum_{j\geq 0} \lambda_j^m (\varphi_j(x) - \varphi_j(y))^2.$$

For more details on the diffusion metric see [9].

The embedding generated by the eigenfunctions can be used for the dimensionality reduction of the data. For a given accuracy δ we retain only the eigenvalues $\lambda_0, ..., \lambda_{p-1}$ that when raised to the power m, exceed a certain threshold (related to delta) and we use the corresponding eigenfunctions $\varphi_0, \varphi_1, ..., \varphi_{p-1}$ to embed the data points in R^p.

III. Comparison of data sets and sensor fusion

The basic idea behind the comparison of data set using diffusion map approach is adopted from [20]. Results in [17] have address the problem of comparison of data sets by studying diffusion maps over changing data sets and generalizing diffusion distance for changing data. The goal is to compare intrinsic geometry of the two data set. Let $X = \{x_1, x_2, ..., x_N\}$ and $Y = \{y_1, y_2, ..., y_N\}$ be the two data sets obtained as time series data from experiment or model simulation. We are assuming that the two data sets are of same size as this is the case of interest to us. However, the approach can be extended to the case when data sets are different size [17]. Using time-delayed coordinates we embed the time series data in R^n, where n is sufficiently large. Now we have $N - n$ data points denoted by

$$\bar{X} := \{\bar{x}_1, \bar{x}_2, ..., \bar{x}_{N-n}\}, \;\; \bar{Y} := \{\bar{y}_1, \bar{y}_2, ..., \bar{y}_{N-n}\},$$

where $\bar{x}_k = (x_k, x_{k+1}, ..., x_{k+n-1})$ and $\bar{y}_k = (y_k, y_{k+1}, .., y_{k+n-1})$. We denote the union of these two data sets by $Z = \{\bar{X}, \bar{Y}\}$. In this paper we use the following Gaussian kernel,

$$k(z_k, z_j) = exp\left(-\frac{\parallel z_k - z_j \parallel^2}{\epsilon}\right), \tag{1}$$

The parameter ϵ specifies the size of the neighborhoods defining the local geometry of the data. The smaller the parameter ϵ the faster the exponential decreases and hence the weight function in (1) becomes numerically insignificant as we move away from the center. It is easy to check that the Gaussian kernel satisfies all the properties of the kernel specified in the previous section.

From this kernel we construct the diffusion operator or the diffusion matrix using the procedure outlined in the previous section. Let $\{\varphi_1, \varphi_2, ..., \varphi_{2(N-n)}\}$ be the eigenvectors of the diffusion matrix and $\{\lambda_1, \lambda_2, ..., \lambda_{2(N-n)}\}$ be the corresponding eigenvalues. Retaining only the first p eigenvectors we can embed the data set Z in a p-dimensional Euclidean diffusion space, where $\{\varphi_1, ..., \varphi_p\}$ are the coordinates of the data points in the Euclidean space. Note that typically $p << n$ and hence we obtain the dimensionality reduction of the original data set. For some index j, the first $N - n$ elements of the eigenvector φ_j are the j-th coordinate in the diffusion space of the $N - n$ data points in X, while the remaining $N - n$ elements are the j-th coordinate in the diffusion space of the data set Y. Denote the eigenvector on data set X by φ^X and data set Y by φ^Y. So we have

$$\varphi := \begin{bmatrix} \varphi^X \\ \varphi^Y \end{bmatrix}.$$

Note that the k-th elements of the j-th eigenvectors are given, respectively, by

$$\varphi_{kj}^X := \varphi_j^X(\bar{x}_k), \;\; \varphi_{kj}^Y := \varphi_j^Y(\bar{y}_k). \tag{2}$$

Now we can use various metric for the comparison of data set

in diffusion space using the above eigenvectors. We define,

$$\phi_k^X = \left(\sum_{j=1}^{p} \lambda_j (\varphi_{kj}^X)^2\right)^{\frac{1}{2}}, \ \phi_k^Y = \left(\sum_{j=1}^{p} \lambda_j (\varphi_{kj}^Y)^2\right)^{\frac{1}{2}} \quad (3)$$

We propose following metric for the comparison of data set.

1) *Weighted average diffusion distance*

$$D_{avg} = \left[\frac{1}{N-n}\sum_{k=1}^{N-n} \phi_k^X\right] - \left[\frac{1}{M-n}\sum_{k=1}^{M-n} \phi_k^Y\right] \quad (4)$$

2) *Pointwise diffusion distance*

$$D_p = \frac{1}{N}\sum_{k=1}^{N} \frac{\left|\phi_k^X - \phi_k^Y\right|}{\phi_k^X}. \quad (5)$$

This metric is sensitive to the ordering of the data set. Other metric can also be constructed depending upon application [21]. For our proposed application of damage diagnosis of wind turbine blades, we employ the pointwise distance for data comparison in diffusion space. The pointwise distance metric gives us satisfactory results. The proposed approach for the comparison of two data sets can be extended to multiple data sets in a straight forward manner [20]. For our proposed application, the different data sets will correspond to the different damage level for wind turbine blades. While the above procedure help us compare different data sets corresponding to different damage level, the procedure can be extended for comparison of data sets from multiple sensors. This can be accomplished using sensor fusion. We consider the case where the wind turbine blade is equipped with an array of distributed sensors. The goal is to fuse the data from multiple sensors for damage diagnosis and also for damage localization.

A. Multiple sensor fusion

In [22], the authors have described the procedure for sensor fusion using diffusion maps. The basic idea behind the sensor fusion using diffusion map is to construct hierarchy of diffusion maps. The algorithm for the multiple sensor fusion as it applies to our problem of damage detection is outlined in Table I. The algorithm closely follows one used in [15] except for the comparison metric that is defined above in Eq. (5). For the simplicity of presentation, we will only consider the case for data fusion from three sensors.

TABLE I: Algorithm for multiple sensor fusion

Comparison of different damage data sets using multiple sensors
1) Let $X_i = \{x_1^i, x_2^i, \ldots, x_N^i\}$, $Y_i = \{y_1^i, y_2^i, \ldots, y_N^i\}$, and $Z_i = \{z_1^i, z_2^i, \ldots, z_N^i\}$ be the data sets from three sensors. The index $i = 0, 1, 2, 3...$ is the index for damage, with 0 is for undamaged case and N is the length of each data set. Using time delayed coordinates,we embed X_i for each i in $\mathbb{R}^n$ where n is sufficiently large. We have $N - n$ data points for individual time series
2) $\bar{X}_i := \{\bar{x}_1^i, \bar{x}_2^i, \ldots, \bar{x}_N^i\}$ where $\bar{x}_k^i = (x_k^i, x_{k+1}^i, \ldots, x_{k+n-1}^i)$
3) We denote the union of these data sets $\bar{X}_0, \bar{X}_1, \ldots$ as $\hat{X} = \{\bar{X}_0, \bar{X}_1, \ldots\}$
4) Applying the procedure outlined above to other sensors Y, Z, we get $\hat{Y}$ and $\hat{Z}$
5) We apply the diffusion map to the data set $\hat{X}$. The embedding coordinates of $\hat{X}$ are scaled and are denoted by Ψ_1 as $\Psi_1(x) = (\frac{\lambda_1\psi_1(x)}{\|\lambda_1\psi_1(x)\|}, \frac{\lambda_2\psi_2(x)}{\|\lambda_2\psi_2(x)\|}, \frac{\lambda_3\psi_3(x)}{\|\lambda_3\psi_3(x)\|}, \ldots)$
6) We repeat the above procedure for all the different data sets $\hat{Y}$ and $\hat{Z}$ and the scaled embedding coordinates for $\hat{Y}$ and $\hat{Z}$ is given by Ψ_2 and Ψ_3.
7) The scaled diffusion coordinates are combined into a matrix form given by $W = \{\Psi_1, \Psi_2, \Psi_3\}$.The diffusion map is applied again on this matrix W.
8) We retain only the first p eigenvectors $(p << n)$ of the diffusion matrix and $\{\lambda_1, \lambda_1, \ldots, \lambda_p\}$ be the corresponding eigen values, so that we can embed the data set W in a p-dimensional Euclidean diffusion space.
9) The eigenvectors obtained can be decomposed according to damage index as $\hat{\varphi} = [\hat{\varphi}^0; \hat{\varphi}^1; \hat{\varphi}^2; \ldots]$
10) The pointwise diffusion distance is applied on these set of eigenvectors in order to capture the varying degrees of damage in the system.

IV. Wind blade and load modeling

In this section we develop the models for the wind turbine blades and wind load.

A. Wind blade model

The wind turbine blade model consists of a cantilever Timosenko beam with bending and shear deformations, which are typically used as condition assessment features for blades [23], a typical approximation used in modeling of blades. The beam is discretized using a lumped masses m where the ith mass is located at the ith node and is linked by a stiffness element k_i and a dashpot element c_i to the $i-1$th mass for all N masses, as shown in Fig. 1. The corresponding degrees-of-freedom x_i, y_i, and θ_i represent the horizontal displacement (longitudinal to the blade), vertical displacement, and rotation of mass, respectively. Each mass is subjected to a load p_i.

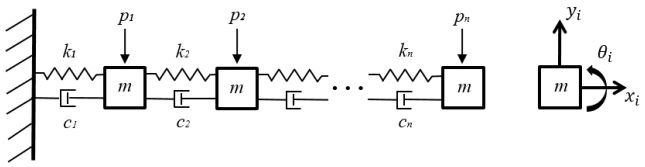

Fig. 1: Lumped mass model

The equation of motion governing the dynamic system is

$$\mathbf{M}\ddot{\mathbf{z}} + \mathbf{C}\dot{\mathbf{z}} + \mathbf{K}\mathbf{z} = \mathbf{P} \tag{6}$$

where $\mathbf{z}$ is the state vector with $\mathbf{z}_i = [x_i, y_i, \theta_i]^T$, $\mathbf{P}$ is the load vector, and $\mathbf{M}$, $\mathbf{C}$, $\mathbf{K}$ are the mass, stiffness and damping matrices, respectively. The assembly of $\mathbf{M}$ and $\mathbf{K}$ is based on the Timoshenko beam element theory, as illustrated in [24], and includes shear and torsional deformations. The model properties include member length L, cross-section width d, thickness t, mass M, Young's modulus E and the shear modulus G. These various model parameter values are provided in Table II(a). The damping matrix $\mathbf{C}$ can be constructed similarly to $\mathbf{K}$. Here, $\mathbf{C}$ is taken as proportional to $\mathbf{K}$ where

$$\mathbf{C} = \alpha\mathbf{K}. \tag{7}$$

Damage is simulated by reducing the stiffness between two nodes and adjusting $\mathbf{C}$ using Eq. (7). We simulate damage that results in a loss of stiffness (from a crack or delamination for instance), a damage mode commonly studied in wind turbine blade literature [5]. This is done in the numerical model by reducing the stiffness k of the element linking node i to node $i+1$. For simulations, we consider damages with loss of 5%, 10%, 15%, 20%, 25% and 30% of stiffness. We assume that strain gauge sensors are distributed on the wind blades. Strain gauge data is simulated on the top surface of the blade. Assuming a rectangular cross-section, surface strain ε_i at location i is taken as $\varepsilon_i = \kappa_i \frac{t}{2}$ where κ_i is the curvature. Assuming small deformations, the curvature can be approximated as follows:

$$\kappa_i = \frac{\tan(\theta_i) - \tan(\theta_{i-1})}{l} \approx \frac{\theta_i - \theta_{i-1}}{l} \tag{8}$$

The numerical model consists of a 23.3m wind turbine blade based on the description provided in [25]. For simplicity of the simulation, a constant cross-section was selected to give equivalent modal properties to dominant modes. The system is discretized into 48 elements giving constant section length $l = 0.48$m and mass $m = 862.5$kg.

TABLE II: Blade and Wind Model parameters.

(a) Model parameters

Parameter	Value
L	23.30 m
d	1.50 m
t	0.50 m
M	4.14×10^4 kg
E	3.57×10^{10} N/m^2
G	2.81×10^9 N/m^2

(b) Wind Model parameters

Parameter	Value
$T_{sr} = T_{sg}$	50 s
T_{er}	350 s
T_{eg}	150 s
h	70 m
A_{ramp}	4 m/s
A_{gust}	-3 m/s
l	600 m
z	0.01m
A_{surf}	36 m^2
W_a	11.5 m/s

B. Wind Load model

The simulated wind load $\mathbf{P}(t) = (p_1(t), \ldots, p_N(t))^T$ acting on the blade is taken as a uniform time-varying load ($p_i(t) = p(t) \quad \forall\, i$). The model for wind speed is taken from [26]. The wind speed model, W_s, consists of four components,

$$W_s = W_a + W_r + W_g + W_t \tag{9}$$

where W_a is the average speed, W_r is the ramp component, W_g models the gust component of wind, and W_t models the turbulence. Following model is used for modeling the ramp component, W_r,

$$W_r = \begin{cases} 0 & \text{if} \quad t < T_{sr} \\ w_{ramp} & \text{if} \quad T_{sr} < t < T_{er} \\ 0 & \text{if} \quad t > T_{er} \end{cases} \tag{10}$$

where $w_{ramp} = A_{ramp}\frac{(t-T_{sr})}{(T_{er}-T_{sr})}$ with A_{ramp} being the amplitude of wind speed ramp, T_{sr} and T_{er} are the starting and end time of wind speed ramp respectively. The model of wind gust, W_g, is assumed to be

$$W_g = \begin{cases} 0 & \text{if} \quad t < T_{sg} \\ w_{gust} & \text{if} \quad T_{sg} < t < T_{eg} \\ 0 & \text{if} \quad t > T_{eg} \end{cases} \tag{11}$$

where, $w_{gust} = A_{gust}\{1 - \cos(2\pi(\frac{t-T_{sg}}{T_{eg}-T_{sg}}))\}$ with A_{gust} being the amplitude of wind gust, T_{sg} and T_{eg} are the starting and end time of wind gust respectively. W_t is modeled as a one dimensional random process and is characterized by the following power spectral density function, $P(f)$ [26]

$$P(f) = lW_a\left(\ln\left(\frac{h}{z_0}\right)^2\right)^{-1}\left(1 + 1.5\frac{fl}{W_a}\right)^{-5/3}$$

$P(f)$ is the power spectral density of the turbulence for a given frequency f, h is the height at which the wind speed is calculated, l is the turbulence length scale, and z_0 is the roughness length. The wind load is directly obtained from W_s using following formula [27]

$$W_F = \rho A_{\text{surf}} C_d \tag{12}$$

where ρ is the dynamic pressure given by $\rho = 0.612W_S^2$, A_{surf} is the surface area and C_d is drag coefficient. Following parameter values are given in Table II(b) which are used in the generation of two different realization of wind speed as shown in Fig. 2.

V. Simulation results

The diffusion map is constructed using the time-series strain output data from the model. We consider three different locations for sensors and damage along the beam. In particular, the damage, $\mathcal{D}$, and sensors, $\mathcal{S}$, are assumed to be located on element $1, 24$, and 48. These element numbers corresponds to root, midsection, and end locations of the beam. We will use the notations $\mathcal{D}_1, \mathcal{D}_{24}, \mathcal{D}_{48}$ and $\mathcal{S}_1, \mathcal{S}_{24}, \mathcal{S}_{48}$ to denote the locations for damage and sensors respectively. The schematic of locations for the damage and sensors is shown in Fig. 3. In the following, we present simulation results for wind load model. Wind turbines blades are normally subjected to highly varying wind loads. In order to simulate the system subjected to such random

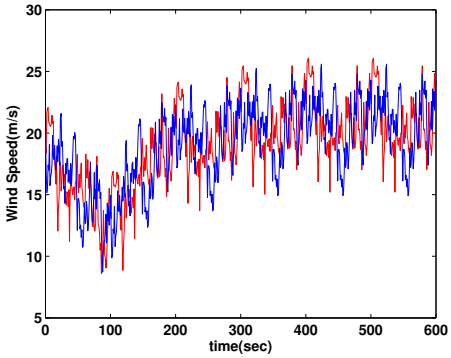

Fig. 2: Two different realization of wind speed.

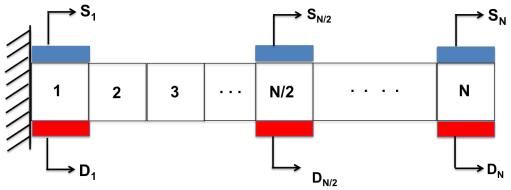

Fig. 3: Schematic showing the location of sensors $\mathcal{S}_1, \mathcal{S}_{24}, \mathcal{S}_{48}$ and element damage $\mathcal{D}_1, \mathcal{D}_{24}, \mathcal{D}_{48}$.

load, the wind load has been generated using the procedure described in section IV-B. We have simulated the model using multiple realizations of wind load for different damage cases. Furthermore, we present analysis using single sensor and sensor fusion involving multiple sensors.

A. Analysis using single sensor

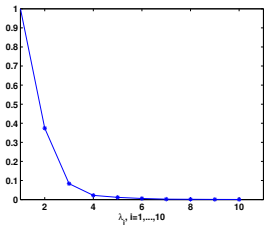

Fig. 4: Eigenvalues

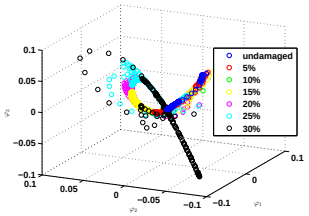

Fig. 5: Three dimensional embedding

In Fig. 4, we show a representative plot for the eigenvalues of diffusion map. We can see that other than the eigenvalue at one, the plot shows that there are three dominant eigenvalues. Hence, the data set can be approximated using three dominant eigenvectors of the diffusion map. Eigenvector plot corresponding to first three dominant eigenvalues for all the damage cases is shown in Fig. 5. In Fig. 6, we show pointwise diffusion distance corresponding to sensor location at element 1 and damage at locations $1, 24$ and 48. It is important to state that the system with different degree of damage is subjected to different realization of wind load. The pointwise diffusion distance shows clear trend where the distance increase with the increase in the percentage of

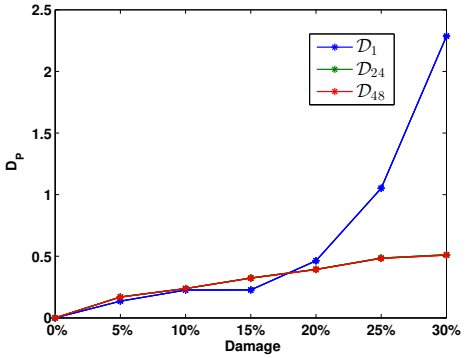

Fig. 6: Pointwise diffusion distance plot for the sensor at S_1 and damage at elements $(\mathcal{D}_1, \mathcal{D}_{24}, \mathcal{D}_{48})$.

damage to the structure. Similar trends in diffusion distance were seen for the case of harmonic loading. We did not include the results for harmonic loading because of space constraints. Pointwise diffusion distance plots with sensors at element $\mathcal{S}_i$ and damage at element $\mathcal{D}_i$ are similar to plot in Fig. 6 for the case when sensor is at element $\mathcal{S}_1$ and damage at element $\mathcal{D}_1$. Furthermore, the pointwise diffusion distance is large when the sensor and damage location coincide and is small for the case where there is a mismatch. This relative sensitivity of diffusion distance with respect to the location of the damage can be used for the purpose of damage localization. This is also confirmed from the plot in Fig. 7. Fig. 7, shows the plot for the pointwise diffusion distance for a fixed damage location at element 1 and sensors at locations $1, 24$, and 48. As seen from this plot the diffusion distance corresponding to sensor location 1 is much larger compared to sensor locations 24 and 48.

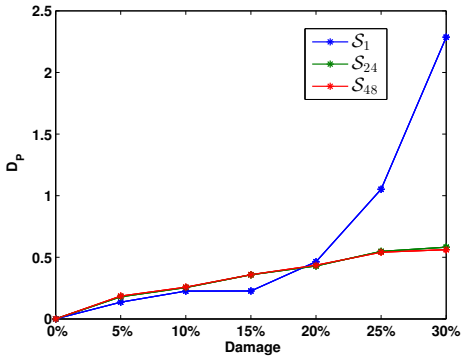

Fig. 7: Pointwise diffusion distance plot for the sensor at element $(\mathcal{S}_1, \mathcal{S}_{24}, \mathcal{S}_{48})$ and damage at $\mathcal{D}_1$.

B. Analysis using multiple sensors

We employ the sensor fusion scheme where data from multiple sensors is used for calculating the pointwise diffusion distance. From Fig. 8 it can be seen that the pointwise diffusion distance increases as we increase the damage in the system. Since the location of damage is not known aprior, the proposed sensor fusion-based pointwise diffusion distance will allow us to overcome the problem associated

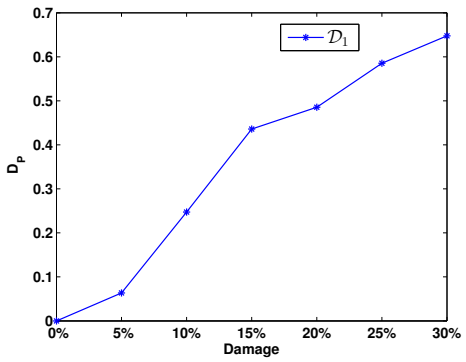

Fig. 8: Poitnwise diffusion distance plot for sensor fusion with sensors at element $(\mathcal{S}_1, \mathcal{S}_{24}, \mathcal{S}_{48})$ and damage at $\mathcal{D}_1$.

with the relative sensitivity of pointwise diffusion distance to the sensor and damage locations.

VI. Conclusion

In this paper, we proposed the application of spectral diffusion map-based approach for structural health monitoring of wind turbine blades. An algorithm has been provided for the comparison of different data set corresponding to different damage level of the blades using pointwise diffusion distance. Similarly, an algorithm for data fusion from multiple sensors is provided for the detection of damage. The simulation results shows that the proposed approach can be used for damage detection and also for determining the extent of the damage. Furthermore, it can be used for the localization of damage. The relative sensitivity of diffusion distance with respect to damage location can also be exploited for the purpose of damage localization.

Acknowledgements

This work is supported by grant 13-02 from the Iowa Energy Center; their support is gratefully acknowledged.

References

[1] C. R. Farrar and N. A. Lieven, "Damage prognosis: the future of structural health monitoring," *Philosophical Transactions of the Royal Society A: Mathematical, Physical and Engineering Sciences*, vol. 365, no. 1851, pp. 623–632, 2007.

[2] S. Laflamme, M. Kollosche, J. J. Connor, and G. Kofod, "Robust flexible capacitive surface sensor for structural health monitoring applications," *Journal of Engineering Mechanics*, vol. 139, no. 7, pp. 879–885, 2012.

[3] P. C. Chang, A. Flatau, and S. Liu, "Review paper: health monitoring of civil infrastructure," *Structural health monitoring*, vol. 2, no. 3, pp. 257–267, 2003.

[4] C. C. Ciang, J.-R. Lee, and H.-J. Bang, "Structural health monitoring for a wind turbine system: a review of damage detection methods," *Measurement Science and Technology*, vol. 19, no. 12, p. 122001, 2008.

[5] D. Adams, J. White, M. Rumsey, and C. Farrar, "Structural health monitoring of wind turbines: method and application to a hawt," *Wind Energy*, vol. 14, no. 4, pp. 603–623, 2011.

[6] S. Laflamme, H. S. Saleem, B. K. Vasan, R. L. Geiger, D. Chen, M. R. Kessler, and K. Rajan, "Soft elastomeric capacitor network for strain sensing over large surfaces," 2013.

[7] F. Ubertini, S. Laflamme, H. Ceylan, A. L. Materazzi, G. Cerni, H. Saleem, A. DAlessandro, and A. Corradini, "Novel nanocomposite technologies for dynamic monitoring of structures: a comparison between cement-based embeddable and soft elastomeric surface sensors," *Smart Materials and Structures*, vol. 23, no. 4, p. 045023, 2014.

[8] B. Glisic and N. Verma, "Very dense arrays of sensors for shm based on large area electronics," *Structural Health Monitoring*, pp. 1409–1416, 2011.

[9] R. R. Coifman, S. Lafon, A. B. Lee, M. Maggioni, B. Nadler, F. Warner, and S. W. Zucker, "Geometric diffusions as a tool for harmonic analysis and structure definition of data: Diffusion maps," *Proceedings of the National Academy of Sciences of the United States of America*, vol. 102, no. 21, pp. 7426–7431, 2005.

[10] L. Moniz, J. Nichols, C. Nichols, M. Seaver, S. Trickey, M. Todd, L. Pecora, and L. Virgin, "A multivariate, attractor-based approach to structural health monitoring," *Journal of Sound and Vibration*, vol. 283, no. 1-2, pp. 295–310, 2005.

[11] L. Overbey, C. Olson, and M. Todd, "A parametric investigation of state-space-based prediction error methods with stochastic excitation for structural health monitoring," *Smart Materials and Structures*, vol. 16, pp. 1621–1638, 2007.

[12] E. Monroig, *Detection of Changes in Dynamical Systems by Nonlinear Time Series Analysis*. PhD thesis, University of Tokyo, 2009.

[13] E. Figueiredo, M. Todd, C. Farrar, and E. Flynn, "Autoregressive modeling with state-space embedding vectors for damage detection under operational variability," *International Journal of Engineering Science*, vol. 48, no. 10, pp. 822–834, 2010.

[14] G. Liu, Z. Mao, M. D. Todd, and Z. Huang, "Damage assessment with state-space embedding strategy and singular value decomposition under stochastic excitation," *Structural Health Monitoring*, p. 1475921713513973, 2013.

[15] N. Rabin and A. Averbuch, "Detection of anomaly trends in dynamically evolving systems.," in *AAAI Fall Symposium: Manifold Learning and Its Applications*, 2010.

[16] Y. Huang, X. F. Zha, J. Lee, and C. Liu, "Discriminant diffusion maps analysis: A robust manifold learner for dimensionality reduction and its applications in machine condition monitoring and fault diagnosis," *Mechanical Systems and Signal Processing*, vol. 34, no. 1, pp. 277–297, 2013.

[17] R. R. Coifman and M. J. Hirn, "Diffusion maps for changing data," *Applied and Computational Harmonic Analysis*, vol. 36, no. 1, pp. 79–107, 2014.

[18] S. S. Lafon, *Diffusion maps and geometric harmonics*. PhD thesis, Yale University, 2004.

[19] F. R. Chung, *Spectral graph theory*, vol. 92. American Mathematical Soc., 1997.

[20] U. Vaidya, G. Hagen, A. Banaszuk, S. Lafon, I. Mezic, and R. R. Coifman, "Comparison of systems using diffusion maps," in *Decision and Control, 2005 and 2005 European Control Conference. CDC-ECC'05. 44th IEEE Conference on*, pp. 7931–7936, IEEE, 2005.

[21] R. Moeckel and B. Murray, "Measuring the distance between time series," *Physica D: Nonlinear Phenomena*, vol. 102, no. 3, pp. 187–194, 1997.

[22] Y. Keller, R. R. Coifman, S. Lafon, and S. W. Zucker, "Audio-visual group recognition using diffusion maps," *Signal Processing, IEEE Transactions on*, vol. 58, no. 1, pp. 403–413, 2010.

[23] H. Kooijman, *Bending-torsion coupling of a wind turbine rotor blade*. Netherlands Energy Research Foundation ECN, 1996.

[24] J. Connor and S. Laflamme, *Structural Motion Engineering*. Springer, 2014.

[25] C. Kong, J. Bang, and Y. Sugiyama, "Structural investigation of composite wind turbine blade considering various load cases and fatigue life," *Energy*, vol. 30, no. 11, pp. 2101–2114, 2005.

[26] T. Ackermann *et al.*, *Wind power in power systems*, vol. 140. Wiley Online Library, 2005.

[27] C. Van der Woude and S. Narasimhan, "Dynamic structural modelling of wind turbines using comsol multiphysics," 2010.